DOI: 10.61782/fa.2023.0427

forum acusticum 2023

A SPHERICAL-HARMONIC-BASED FRAMEWORK FOR SPATIAL SAMPLING CONSIDERATIONS OF MUSICAL INSTRUMENT AND VOICE DIRECTIVITY MEASUREMENTS

Samuel D. Bellows[1*] **Timothy W. Leishman**[1]
[1] Acoustics Research Group, Department of Physics and Astronomy, Brigham Young University, USA

ABSTRACT

Researchers have employed numerous array configurations and sampling densities to thoroughly measure the sound radiations of live sources, such as musical instruments and speech. The number of sampling positions has varied from fewer than a hundred to over a thousand, with measurement inconsistencies highlighting a knowledge gap in the number of sampling positions required for spherical directivity measurements. This work presents theoretical methods and practical metrics to assess the required number of sampling positions for a given source to mitigate spatial aliasing. Theoretical developments show that the number of necessary sampling positions closely relates to source geometry due to the spatial filtering effects of far-field propagation. Initial results from theoretical models generalize the approach to live sources.

Keywords: *directivity, sampling, musical instruments, speech*

1. INTRODUCTION

Acoustic directivity measurements are essential tools for establishing the radiation patterns of sources. Their data have applications in room acoustical design [1, 2], auralizations [3, 4], microphone placements [5–7], sound source modeling [8, 9], and other areas. Despite the significance of these data, the number of discrete sampling positions employed for published measurements has varied dramatically from fewer than a hundred [10–13] to well over a thousand [14–17]. Meanwhile, Audio Engineering Society (AES)-standardized directivity measurements with 10° and 5° dual-equiangular resolutions [14] have become ubiquitous for loudspeaker assessments and room-acoustical simulation software [18, 19]. Nevertheless, the standard provides little guidance on the maximum usable frequency for a given source using either resolution. Furthermore, sampling inconsistencies between published works highlight ambiguities regarding the most suitable number of sampling positions for effective directivity measurements.

Researchers have long applied spherical harmonic expansions of measured acoustic pressures for directivity applications [12, 20]. The expansions serve as the angular component of the Helmholtz equation's solution in spherical coordinates [21] and allow continuous, rather than discrete, representations of the pressure fields. Previous works have identified relations between the number of discretely sampled positions and the maximum spherical harmonic degree feasible in such expansions without significant spatial aliasing effects [22]. Other works have sought to relate source geometry and other properties to the maximum degree required for source representations, e.g., through multipole expansions [20, 23]. However, researchers and practitioners will benefit from additional and more concrete developments, including methods to determine limiting frequencies due to spatial aliasing. An improved understanding of such sampling considerations will enable them to make more successful directivity measurements.

This work approaches spatial sampling by considering the effect of far-field propagation on a source's radi-

*__Corresponding author__: samuel.bellows11@gmail.com.

ated pressure spectrum. Sound radiation theory demonstrates that far-field propagation behaves as a frequency-dependent low-pass spatial filter. This model describes the relationship between the maximum spherical harmonic degree and source geometry. Once identified, this degree determines the number of required sampling positions. A method for estimating source order based on measured directivity functions yields a practical tool for users to understand when spatial aliasing limits applications of spherical harmonic expansions. Results for various musical instruments and speech serve as examples of the theory's application for practical cases.

2. THEORETICAL BACKGROUND

2.1 Spherical Harmonic Expansions

Spherical harmonic expansions provide a helpful framework for understanding directivity measurement sampling considerations. Consider a square-integrable function f defined over the sphere so that it may be expanded as [24]

$$f(\theta,\phi) = \sum_{n=0}^{\infty} \sum_{m=-n}^{n} f_n^m Y_n^m(\theta,\phi) \tag{1}$$

where Y_n^m are the spherical harmonics of degree n and order m [25] and f_n^m are the expansion coefficients. Two important characteristics of the spherical harmonics motivate their choice as basis functions. First, as the eigenfunctions of the Laplace-Beltrami operator over the sphere, they serve as the angular component of the solution to the Helmholtz equation in spherical coordinates [21, 26]. As a result, spherical harmonic expansions find application in acoustical and near-field acoustical holography [21], source centering algorithms [27], and other wave-based representations of sound fields [9]. Second, the spherical harmonics form an orthonormal basis for the Hilbert space of square-integrable functions defined over the sphere [24]. This essential feature ensures special convergence properties of spherical harmonic expansions.

Understanding the expansion's convergence is essential because discretely sampling the sphere limits the maximum resolvable expansion degree [22]. Consequently, the pressure field produced by an acoustic source must be band-limited to some maximum degree N to avoid spatial aliasing effects. One approach to evaluate an expansion's convergence is through its norms [28]. From Parseval's identity [24, 26]:

$$\|f(\theta,\phi)\|_{L^2}^2 = \|f_n^m\|_{\ell^2}^2 \tag{2}$$

where

$$\|f(\theta,\phi)\|_{L^2}^2 = \int_0^{2\pi} \int_0^{\pi} |f(\theta,\phi)|^2 \sin\theta d\theta d\phi \tag{3}$$

is the norm in the function space of square-integrable functions L^2 and

$$\|f_n^m\|_{\ell^2}^2 = \sum_{n=0}^{\infty} \sum_{m=-n}^{n} |f_n^m|^2 \tag{4}$$

is the norm in the sequence space of square-summable sequences ℓ^2 [29]. It is convenient to represent the sequence space's norm in terms of the energy per degree metric [24]

$$E_n = \sum_{m=-n}^{n} |f_n^m|^2 \tag{5}$$

so that

$$\|f_n^m\|_{\ell^2}^2 = \sum_{n=0}^{\infty} E_n. \tag{6}$$

The energy per degree represents a function's spherical spectrum, indicating which expansion degrees contain the most "signal energy." While one could consider a spherical spectrum analysis over both degree n and order m, this approach is not considered in this work because the order m of a spherical harmonic closely relates to rotations of degree n polynomials over the sphere [24]. In other words, for a fixed degree n, rotations of the function f "shuffle" energy between the coefficients of different orders m. However, their energetic sum represented by E_n remains constant [24]. Thus, E_n serves as a rotation-invariant metric for spatial-spectral analysis.

Next, defining a truncation parameter as

$$\gamma(N) = \frac{\sum_{n=0}^{N} E_n}{\sum_{n=0}^{\infty} E_n} \tag{7}$$

provides a means to monitor the convergence of an expansion over increasing truncation degree N. Clearly, as $N \to \infty$, $\gamma \to 1$. Additionally, because $E_n \geq 0$ [See Eq. (5)], the sequence defined by γ monotonically increases. Although many practical sources are not truly band-limited, they may behave approximately so. Evaluating the rate of convergence of γ allows one to quantify when a function sufficiently behaves as band-limited. For

example, increasing N until γ surpasses a value of 0.98 ensures that the exclusion of coefficients with $n > N$ loses no more than 0.1 dB of signal energy.

A simple theoretical source distribution illustrates these convergence trends. A spherical cap function [22, 30] finds use in applications such as estimating radiation from loudspeakers [30, 31], horns [32], and speech [17]. Figure 1(a) plots the energy per degree E_n on a logarithmic scale for a spherical cap with cap half-angle $\theta_0 = 30°$. The spectrum reveals that the most significant expansion coefficients fall within $0 \leq n \leq 10$. Additionally, the relative contribution of expansion coefficients with $n > 50$ has decayed to over 20 dB down from the maximum. Figure 1(b) plots γ over increasing truncation degree N. The value of γ quickly exceeds 0.9 by $N = 10$; however, achieving $\gamma = 0.98$ requires an $N = 58$ degree expansion. As a reference, Fig. 1(c) plots the spherical cap function expanded with select N to allow comparisons between increasing values of γ and the converging spherical function. Although the expansion technically requires infinite terms to attain convergence, analysis of E_n and γ provides insight into when the function behaves approximately as band-limited.

2.2 Far-Field Propagation as a Filter

An arbitrary source's spherical spectrum is generally unknown. However, the maximum necessary expansion degree N determines the number of sampling positions needed and relates to the maximum usable frequency for spherical-harmonic-based analysis [22]. Thus, a means to estimate N before measurement would benefit practical directivity measurements. This section shows how far-field relations enable a method for estimating N for a given source based on its geometry.

Consider an acoustic source of maximum radial extent R_s from the origin. If a notional sphere of radius $r = R_s$ encloses the source, then the pressure on this sphere may be expanded as [21]

$$p(R_s, \theta, \phi, k) = \sum_{n=0}^{\infty} \sum_{m=-n}^{n} p_n^m(k) Y_n^m(\theta, \phi) \tag{8}$$

where k is the wavenumber and $p_n^m(k)$ are the frequency-dependent expansion coefficients. Because these expansion coefficients depend on the source, one can infer little about a suitable truncation degree N without measurement or modeling.

For $r > R_s$, the pressure becomes [21]

$$p(r, \theta, \phi, k) = \sum_{n=0}^{\infty} \sum_{m=-n}^{n} \frac{h_n^{(2)}(kr)}{h_n^{(2)}(kR_s)} p_n^m(k) Y_n^m(\theta, \phi) \tag{9}$$

where $h_n^{(2)}$ are the spherical Hankel functions of the second kind of order n. When considering wave propagation from concentric spheres centered about the origin, the quotient

$$G_n(r, k) = \frac{h_n^{(2)}(kr)}{h_n^{(2)}(kR_s)}, \quad r > R_s \tag{10}$$

serves as a "propagator" [21], modifying the pressure observed at radius R_s to that observed at radius r. This propagator behaves as a spatial filter dependent upon the choice of radial observation distance r, spherical Hankel order n, and wavenumber k. Applying the large-argument relation for the spherical Hankel functions [25] yields the far-field result

$$p_{ff}(r, \theta, \phi, k) = \frac{e^{-ikr}}{kr} \sum_{n=0}^{\infty} \sum_{m=-n}^{n} \frac{i^{n+1}}{h_n^{(2)}(kR_s)} p_n^m(k) Y_n^m(\theta, \phi), \tag{11}$$

so that the far-field propagator becomes

$$G_n^{(ff)}(k) = \frac{i^{n+1}}{h_n^{(2)}(kR_s)}. \tag{12}$$

The source's unnormalized far-field directivity function follows as

$$D_{ff}(\theta, \phi, k) = \sum_{n=0}^{\infty} \sum_{m=-n}^{n} a_n^m(k) Y_n^m(\theta, \phi), \tag{13}$$

where

$$a_n^m(k) = G_n^{(ff)}(k) p_n^m(k) \tag{14}$$

are the far-field directivity expansion coefficients.

Because most applications employ far-field directivities, the filtering effect of the far-field propagator is particularly pertinent. Figure 2 plots the energy per degree of $G_n^{(ff)}$ as a function of the Helmholtz number kR_s and expansion degree n. Color indicates the relative level on a 25 dB scale normalized to the maximum value for each frequency. White indicates the most significant coefficients, whereas black indicates the least important coefficients. In this surface plot, a vertical "slice" would map to an energy-per-degree plot similar to Fig. 1(a).

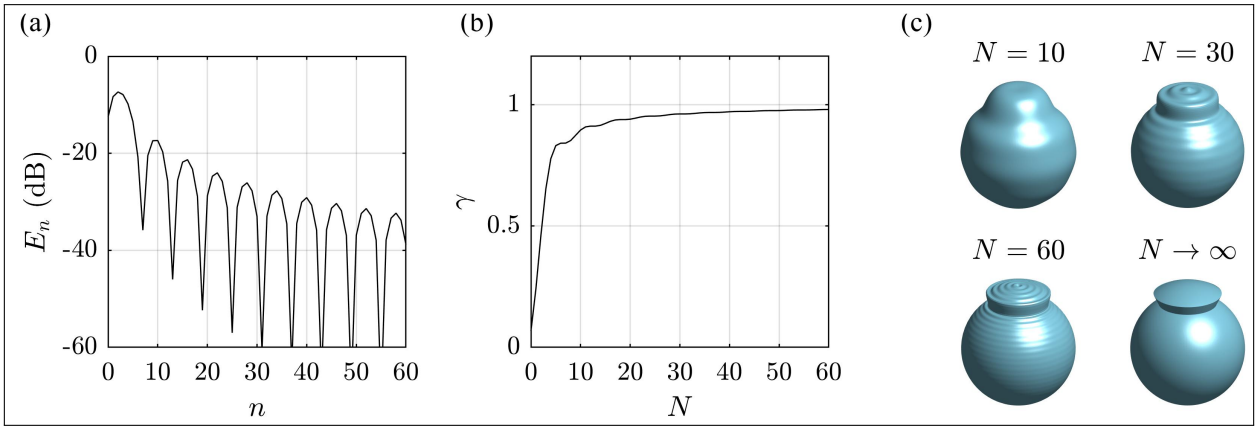

Figure 1. (a) Energy per degree E_n for a spherical cap function with cap half-angle $\theta_0 = 30°$. (b) Truncation parameter γ over increasing maximum expansion degree N. (c) Expansions of the spherical cap function for select N. Similar to Fig. 1.14 of Ref. [22], an added radial offset enhances visualization of the spherical function.

The plotted far-field propagator's spectrum reveals a frequency-dependent, low-pass filtering effect. An overlaid magenta dashed line represents $n = kR_s$, the approximate low-pass filter cut-off. As a result, far-field propagation tends to strongly attenuate the expansion coefficients $p_n^m(k)$ with $n \gtrapprox kR_s$. Consequently, when sampling in the far-field of the source, the relation $N \approx kR_s$ provides an estimate of the maximum necessary N for expansion. This result coincides with Weinreich's observation that a source of maximum dimension R_s requires roughly up to spherical Hankel function order $N \approx kR_s$ for its representation [20]. This maximum N required for sufficient representation is the source order. It is frequency dependent and linearly related to the source geometry.

To further demonstrate the impact of the low-pass filtering effect, Fig. 3 compares the spherical spectrum of the near-field and far-field pressure for a radially vibrating cap on a sphere of radius a with a cap half-angle $\theta_0 = \pi/10$. Figure 3(a) plots the energy per degree for the pressure evaluated at the surface of the radius $R_s = a$ sphere. The pressure's near-field spectrum shows similar lobing effects, evidenced as horizontal bands, to the energy per degree of the spherical cap function seen in Fig. 1(a). Additionally, it is clear that in the near-field, some coefficients with $n > kR_s$ contain essential signal energy.

In contrast, the far-field directivity coefficient's spectrum in Fig. 3(b) demonstrates that far-field propagation filters out the coefficients with $n \gtrapprox kR_s$. Consequently, while it may be challenging to determine the necessary expansion degree for arbitrary sources in the near field, far-field propagation allows one to estimate the required expansion degree based on source geometry. For example, modeling a loudspeaker as this spherical source would require at least an $N = 37$ degree expansion for a dimension of $R_s = a = 0.1$ m and a maximum desired frequency of 20 kHz.

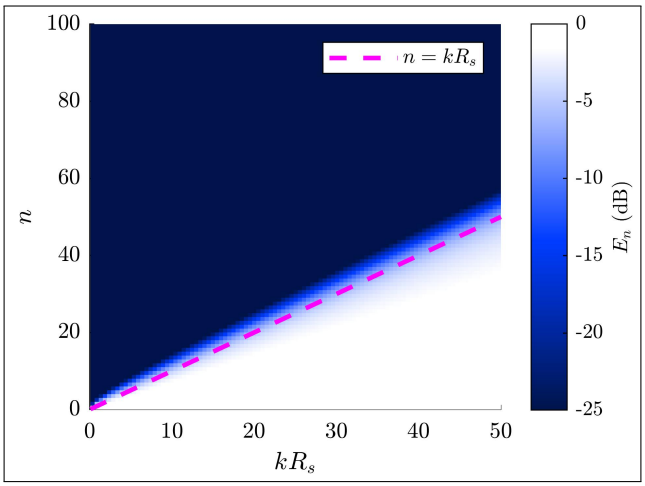

Figure 2. Energy per degree of the far-field propagator $G_n^{(ff)}$ over increasing kR_s.

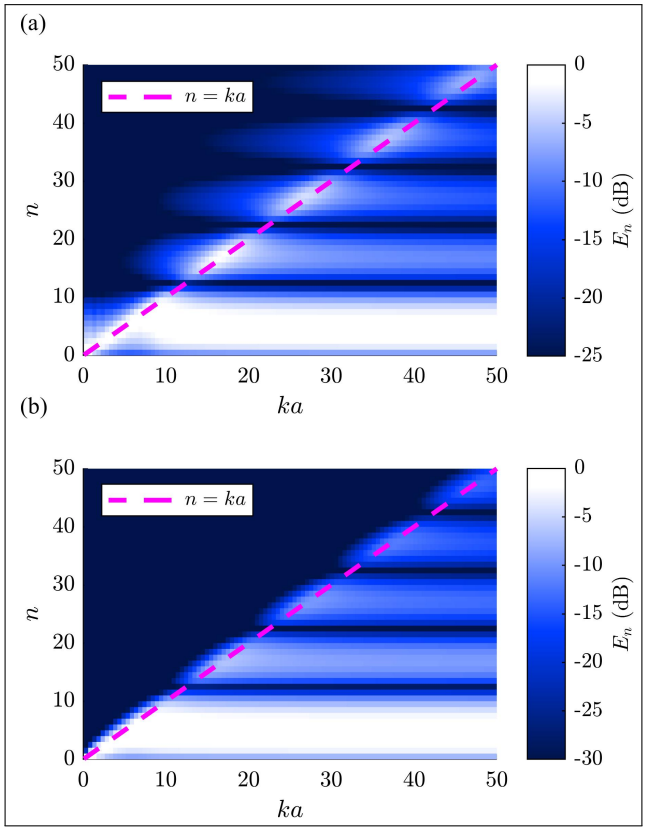

Figure 3. Energy per degree of the pressure produced by a radially vibrating cap on a rigid sphere of radius a, evaluated at two radial distances: (a) on the sphere's surface and (b) in the far field.

2.3 Discrete Sampling Relations

Once estimated for a given source, the source order N determines the necessary number of sampling positions Q. As detailed in Ref. [22], there are numerous approaches to sampling the sphere, such as Gaussian, equiangular, or uniform and quasi-uniform sampling. Each scheme has advantages and disadvantages regarding efficiency and practical implementation; however, they generally follow the trend that $Q \propto (N+1)^2$. For example, a Gaussian sampling scheme can exactly calculate spherical harmonic expansions up to degree $N = \sqrt{Q/2} - 1$ [22]. Continuing the example from Sec. 2.2, a 0.1 m radius spherical model of a loudspeaker would require at least $Q = 2(37+1)^2 = 2,888$ measurement positions configured for Gaussian sampling for spherical-harmonic-based analysis up to 20 kHz. Although the number of measurement positions will vary depending on the sampling configuration, the spherical-harmonic-based framework provides an exact estimate of the required sampling positions for a given spherical harmonic expansion degree N.

3. METHOD FOR ESTIMATING THE EFFECTIVE SOURCE DIMENSION FROM DATA

The simple geometries of theoretical models permit straightforward source-order predictions based on physical arguments. However, there are benefits to determining the source orders of more complexly shaped bodies from measured data, which requires predicting R_s, a source's effective acoustic dimension. Because source order varies roughly linearly with respect to frequency, a least-squares fit to the line $N = kR_s$ can predict R_s based on calculated values of N at select wavenumbers k. These values follow by determining the minimum N necessary to obtain a selected truncation value using Eq. (7), such as $\gamma = 0.98$. Section 4 demonstrates this approach for select musical instruments and voice directivity measurements.

4. RESULTS FOR MEASURED SOURCES

4.1 Musical Instruments

An interesting musical instrument directivity example involves the previously reported radiation from a gamelan ageng lanang gong [33]. Figure 4 shows the gong's spherical spectrum. The overlaid green circles indicate the degree N at which $\gamma = 0.98$ for 35 modal peaks under 1.5 kHz. The overlaid magenta dashed line shows the associated least-squares fit to $N = kR_s$ with $R_s = 0.54$ m. The latter value corresponds well to a rough geometrical estimate for R_s based on the gong's 0.41 m radius and the additional support structures used to suspend the instrument. Assuming a maximum $N = 34$ expansion afforded by the measurement's 5° dual-equiangular sampling scheme would limit spherical harmonic analysis to about 3.4 kHz without spatial aliasing.

4.2 Speech

Because voice directivity is critical for audio, telecommunications, and acoustical room designs, understanding spatial sampling requirements for speech has many practical benefits. Radiation from the human voice is also an interesting case study because sound predominately originates from the mouth, which is significantly smaller than

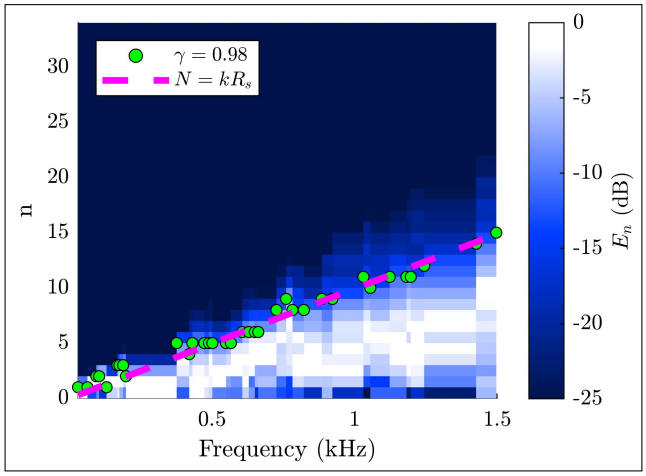

Figure 4. Spherical spectrum of a gamelan ageng lanang gong's far-field directivity.

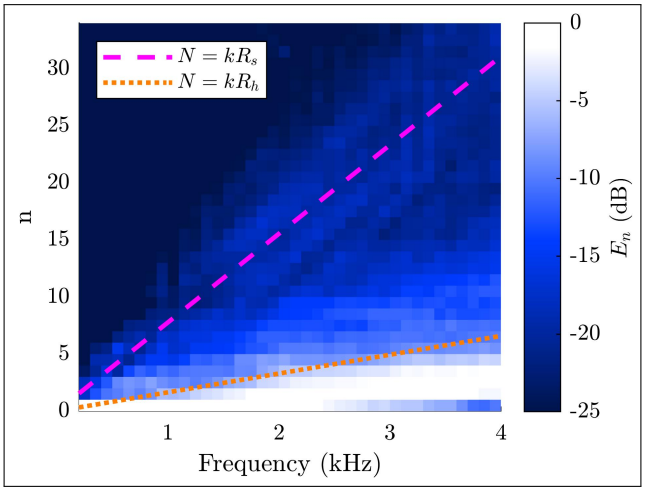

Figure 5. Spherical spectrum of a female talker's measured directivity.

the entire body. Although torso diffraction strongly influences voice directivities [34], it is common to simulate voice radiation using only an isolated mannikin head. These differences lead to an ambiguity of whether the effective source radius R_s should incorporate the entire body or just the head.

Figure 5 plots the spherical spectrum at the measurement radius for a female talker [17]. Interestingly, the spectrum shows a strong white band that does not exceed $n = 5$ by 4 kHz. An overlaid orange dotted line at $N = kR_h$, where $R_h = 0.09$ m represents the approximate head radius, suggests that these highest-magnitude coefficients may relate to the radiation from the mouth and head. The overlaid magenta line indicates the least-squares fit using $\gamma = 0.98$; it corresponds to a source dimension of $R_s = 0.44$ m. This figure agrees much better with rough geometrical approximations considering the average spatial extent of a seated human talker.

Figure 6 compares various narrowband (1 Hz resolution) speech directivity balloons at 500 Hz to explore the impact of neglecting the lower-amplitude coefficients above $n = kR_h$. Figure 6(a) plots the FRF-based directivity acquired from a multiple-capture transfer-function method on the measurement surface [17]. Even at this lower frequency, significantly reduced levels behind the seated talker appear.

The values $k = 9.16$ m^{-1} at 500 Hz and $R_h = 0.09$ m would suggest that $N = \lceil kR_h \rceil = 1$ is sufficient for source representation, where $\lceil\,\rceil$ is the ceiling function. Accordingly, Fig. 6(b) plots the propagated far-field directivity based on an $N = 1$ degree expansion. While the expansion preserves some essential directional characteristics, it loses other crucial details, including the distinctive effects of diffraction and absorption about the seated body and chair.

In contrast, using the full-body source dimension estimate $R_s = 0.44$ m yields $N = \lceil kR_s \rceil = 5$ as the expansion limit for the improved directivity approximation in Fig. 6(c). Finally, Fig. 6(d) plots the far-field propagated directivity based on an $N = 34$ expansion. These final two directivities show much better agreement with the raw data and include the locations of reduced sound levels due to diffraction about the body. The directivity factor deviation function levels [34] between the $N = 34$ degree far-field directivity expansion and the $N = 1$ and $N = 5$ degree expansions are 1.2 dB and 0.5 dB, respectively. From this example, it is apparent that estimating a source's effective dimension requires careful consideration. For $R_s = 0.44$ m, spatial aliasing limits spherical-harmonic analysis on complex-valued narrowband data beyond 4.2 kHz.

5. DISCUSSION AND CONCLUSIONS

Plotting the spherical spectrum of a source is a powerful tool for analyzing sampling limitations and source orders. This work's theoretical and experimental results suggest that an effective acoustic dimension may help characterize

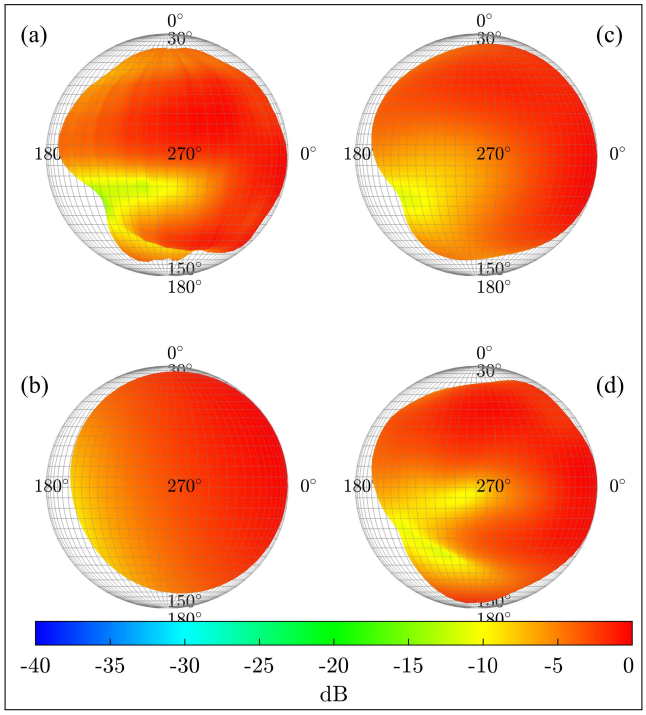

Figure 6. Narrowband female voice directivities at 500 Hz. (a) Measured FRF-based balloon. Far-field directivities based on (b) $N = 1$, (c) $N = 5$, and (d) $N = 34$ degree spherical harmonic expansions.

source order. The presented techniques allow researchers and practitioners to estimate the required number of sampling positions for a given source while highlighting limitations to current sampling standards.

For the sources considered in this work, AES 5° dual-equiangular sampling [14], currently the highest standardized directivity resolution, is often only sufficient to allow spherical-harmonic-based analysis up to a few kilohertz. Comprehensive, spherical-harmonic-based analysis of complex-valued narrowband data over the entire audio bandwidth would require significantly higher sampling density. For example, using the effective source dimension of $R_s = 0.44$ m given in Sec. 4.2, analysis up to 20 kHz ($k \approx 370$ m^{-1}) would require $N \approx 162$ degree expansions. Dual-equiangular sampling with 1° resolution and 64,082 unique positions over a sphere would satisfy this requirement [22, 28]. However, this density would dramatically increase the number of sampling positions used in current sampling standards and practices.

Future work could consider other methods for estimating a source's effective acoustic dimension. Efforts that tabulate these dimensions for common sources would benefit experimentalists in their measurement designs.

6. ACKNOWLEDGMENTS

The authors express appreciation for funding from the William James and Charlene Fuhriman Strong Family Endowed Fellowship Fund for Musical Acoustics.

7. REFERENCES

[1] J. Meyer, "The sound of the orchestra," *J. Audio Eng. Soc.*, vol. 41, pp. 203–213, April 1993.

[2] C. H. Jeong, J. G. Ih, C. H. Yeon, and C. H. Haan, "Prediction of the acoustic performance of a music hall considering the radiation characteristics of korean traditional musical sources," *J. Acoust. Soc. Kr.*, vol. 23, no. 2, pp. 146–161, 2004.

[3] F. Otondo and J. H. Rindel, "The influence of the directivity of musical instruments in a room," *Acta Acustica united with Acustica*, vol. 90, pp. 1178–1184, 2004.

[4] F. Otondo and J. H. Rindel, "A new method for the radiation representation of musical instruments in auralizaitons," *Acta Acustica united with Acustica*, vol. 91, pp. 902–906, 2005.

[5] M. Clark and P. Minter, "Dependence of timbre on the tonal loudness produced by musical instruments," *J. Audio Eng. Soc.*, vol. 12, no. 1, pp. 28–31, 1964.

[6] B. A. Bartlett, "Tonal effects of close microphone placement," *J. Audio Eng. Soc*, vol. 29, pp. 726–738, oct 1981.

[7] S. D. Bellows and T. W. Leishman, "Optimal microphone placement for single-channel sound-power spectrum estimation and reverberation effects," *J. Audio Eng. Soc*, vol. 71, no. 1/2, pp. 20–33, 2023.

[8] J. Escolano, J. J. López, and B. Pueo, "Directive sources in acoustic discrete-time domain simulations based on directivity diagrams," *J. Acoust. Soc. Am.*, vol. 121, no. 6, pp. EL256–EL262, 2007.

[9] S. Bilbao, J. Ahrens, and B. Hamilton, "Incorporating source directivity in wave-based virtual acoustics: Time-domain models and fitting to measured data," *J. Acoust. Soc. Am.*, vol. 146, no. 4, pp. 2692–2703, 2019.

[10] H. Dunn and D. W. Farnsworth, "Exploration of pressure field around the human head during speech," *J. Acoust. Soc. Am.*, vol. 10, pp. 184–199, January 1939.

[11] J. Meyer, *Acoustics and the Performance of Music: Manual for Acousticians, Audio Engineers, Musicians, Architects, and Musical Instrument Makers*. New York, New York: Springer Science+Business Media, 5 ed., 2009.

[12] F. Zotter, "Analysis and synthesis of sound-radiation with spherical arrays," *Doctoral Dissertation, Institute of Electronic Music and Acoustics University of Music and Performing Arts*, 2009.

[13] N. R. Shabtai, G. Behler, M. Vorländer, and S. Weinzierl, "Generation and analysis of an acoustic radiation pattern database for forty-one musical instruments," *J. Acoust. Soc. Am.*, vol. 141, no. 2, pp. 1246–1256, 2017.

[14] *AES56-2008 (r2019): AES standard on acoustics - Sound source modeling - Loudspeaker polar radiation measurments*. New York, New York: Audio Engineering Society, August 2019.

[15] K. J. Bodon, "Development, evaluation, and validation of a high-resolution directivity measurement system for played musical instruments," *Master's thesis, Brigham Young University*, 2016.

[16] T. Grothe and M. Kob, "High resolution 3D radiation measurements on the bassoon," in *Proceedings ISMA*, (Detmold, Germany), pp. 139–145, 2019.

[17] T. W. Leishman, S. D. Bellows, C. M. Pincock, and J. K. Whiting, "High-resolution spherical directivity of live speech from a multiple-capture transfer function method," *J. Acoust. Soc. Am.*, vol. 149, no. 3, pp. 1507–1523, 2021.

[18] CLF Group, "CLF: A common loudspeaker format," *Syn-Aud-Con Newsl.*, vol. 32, pp. 14–17, 2004.

[19] *GLL Loudspeaker File Format*. Ahnert Feistel Media Group, 2021.

[20] G. Weinreich, "Sound hole sum rule and the dipole moment of the violin," *J. Acoust. Soc. Am.*, vol. 77, no. 2, pp. 710–718, 1985.

[21] E. G. Williams, *Fourier Acoustics: Sound Radiation and Nearfield Acoustical Holography*. London: Academic Press, 1999.

[22] B. Rafaely, *Fundamentals of Spherical Array Processing*, vol. 8. Berlin Heidelberg: Springer-Verlag, 2015.

[23] A. D. Pierce, *Acoustics*. Springer International Publishing, 2019.

[24] R. Kennedy and P. Sadeghi, *Hilbert Space Methods in Signal Processing*. Cambridge University Press, 2013.

[25] T. M. Dunster, *NIST Handbook of Mathematical Functions*. New York: Cambridge University Press, 2010.

[26] S. Hassani, *Mathematical Physics: A Modern Introduction to Its Foundations*. Springer, 2 ed., 2013.

[27] I. Ben Hagai, M. Pollow, M. Vorländer, and B. Rafaely, "Acoustic centering of sources measured by surrounding spherical microphone arrays," *J. Acoust. Soc. Am.*, vol. 130, no. 4, pp. 2003–2015, 2011.

[28] S. D. Bellows and T. W. Leishman, "Spherical harmonic expansions of high-resolution musical instrument directivities," *Proc. Mtgs. Acoust. 35, 035005*, 2018.

[29] M. C. Pereyra and L. A. Ward, *Harmonic Analysis: From Fourier to Wavelets*. American Mathematical Society, 2012.

[30] L. Beranek and T. Mellow, *Acoustics: Sound fields, transducers and vibration*. Academic Press, 2 ed., 2019.

[31] R. M. Aarts and A. J. E. M. Janssen, "Comparing sound radiation from a loudspeaker with that from a flexible spherical cap on a rigid sphere," *J. Audio Eng. Soc.*, vol. 59, p. 201, 2011.

[32] T. Hélie and X. Rodet, "Radiation of a pulsating portion of a sphere: Application to horn radiation," *Acta Acustica united with Acustica*, vol. 89, no. 4, pp. 565–577, 2003.

[33] S. D. Bellows, D. T. Harwood, K. L. Gee, and T. W. Leishman, "Low-frequency directional characteristics of a gamelan gong," *Proc. Mtgs. Acoust.*, vol. 50, no. 1, p. 035003, 2022.

[34] S. Bellows and T. W. Leishman, "Effect of Head Orientation on Speech Directivity," in *Proc. Interspeech 2022*, pp. 246–250, 2022.